Intelligent acoustic-based fault diagnosis of roller bearings using a deep graph convolutional network

Dingcheng Zhang [a,*], Edward Stewart [a], Mani Entezami [a], Clive Roberts [a], Dejie Yu [b]

[a] School of Engineering, University of Birmingham, Birmingham B152TT, United Kingdom
[b] State Key Laboratory of Advanced Design and Manufacturing for Vehicle Body, Hunan University, Changsha 410082, China

ARTICLE INFO

ABSTRACT

Roller bearings form key components in many machines and, as such, their health status can directly influence the operation of the entire machine. Acoustic signals collected from roller bearings contain information on their health status. Hence, acoustic-based fault diagnosis techniques can provide novel solutions as condition monitoring tools for roller bearings. Traditionally, acoustic fault diagnosis methods have been based on conventional signal processing methods in which prior expert knowledge has been required in order to extract and interpret the health information contained within the collected acoustic signals. As an alternative, deep learning methods can be used to obtain heath information from the collected signals by constructing 'end-to-end' models that do not rely on prior knowledge. These approaches have been successfully applied in the condition monitoring of industrial machinery. However, conventional deep learning methods can only learn features from the vertices of input data and thereby ignore the information contained in the relationships (edges) between vertices. In this paper, which combines graph convolution operators, graph coarsening methods, and graph pooling operations; a deep graph convolutional network (DGCN) based on graph theory is applied to deliver acoustic-based fault diagnosis of roller bearings. In the proposed method, the collected acoustic signals are first transformed into graphs with geometric structures. The edge weights represent the similarity between connected vertices, which enriches the input information and hence improves the classification accuracy of the deep learning methods applied. To verify the effectiveness of the proposed system, experiments with roller bearings of varying condition were carried out in the laboratory. The experimental results demonstrate that the DGCN method can be used to detect different kinds and severities of faults in roller bearings by learning from the constructed graphs. The results have been compared to those obtained using other, conventional, deep learning methods applied to the same datasets. These comparative tests demonstrate improved classification accuracy when using the DGCN method.

© 2020 Elsevier Ltd. All rights reserved.

1. Introduction

Roller bearings play an important role in industry and are widely used in many different kinds of machines. Roller bearings often carry substantial loads and may even support the whole weight of the machines of which they are part. Under these conditions, it is possible for faults to develop and for those faults to have significant potential consequences. In order to avoid failures, maintenance of bearings and bearing components tends to be preventative, but this can lead to over-maintenance and inefficiency. In order to reduce costs and maximise the availability of machines, condition monitoring of bearings is an increasingly popular approach, and a vital step towards condition-based maintenance. Acoustic-based fault diagnosis is one such monitoring technique; it involves analysis of acoustic signals collected from microphones. The technique has been applied to many systems, such as railway bridges [1], gearboxes [2], motors [3], etc. Acoustic-based fault diagnosis has also successfully been applied to roller bearings [4,5].

In acoustic-based fault diagnosis, microphones are installed adjacent to target bearings. The recorded acoustic signal is then analysed in order to detect faults within those bearings with no requirement for direct access to them in order to install the equipment [5,6]. Hence, acoustic-based fault diagnosis techniques have obvious advantages in terms of practicality and cost when compared to other techniques such as vibration-based or acoustic emission-based approaches. However, acoustic signals normally have high-levels of background noise and may contain acoustic

* Corresponding author.
  E-mail address: railcm@contacts.bham.ac.uk (D. Zhang).

signals generated by other components in the machine. Hence, signal-processing methods are required in order to realise the health analysis benefits. For example: a method considering the amplitude of particular frequencies of the acoustic signals was used to identify fault-features in [4]; and a method combining improved singular value decomposition with resonance-based signal sparse decomposition was proposed in [6]. Conventional signal processing-based methods, such as these, have been shown to achieve good performance in many cases, however, expert knowledge is generally required to support and interpret the results of fault detection systems based on them. Also, each signal sample has to be analysed by signal processing-based methods. It is time-consuming as large volumes of data need to be processed. Furthermore, stochastic factors in the real operating environment will affect the acoustic signals and hence may reduce the effectiveness of these conventional signal processing based methods.

Deep learning (DL) is a powerful machine learning approach which is currently prevalent among machine learning techniques. DL has recently demonstrated strong performance in a number of areas, in particular in condition monitoring applications [7]. DL models can be trained by learning abstract features from massive datasets off-line and then the trained model can be directly used to identify different fault types or fault severities, which are efficiency procedures [8]. Intelligent condition monitoring systems based on DL have successfully been applied to induction motors [9], planetary gearboxes [10], axial piston pumps [11], etc. There is also a range of work focusing on intelligent fault detection of for bearings. For example, Zhang et al. proposed an ensemble DL method combining convolution neural networks (CNN) and a small batch training [12]. In [13], an improved convolutional deep belief network (DBN) was proposed by combining a standard DBN with a compressed sensing technique. The approach also used an exponential moving average method to smooth the weightings in the DL algorithm. Jia et al. proposed a parameter selection strategy for the deep autoencoder (DAE) method in [14]. The deep recurrent neural network (DRNN) constructed from long-short term memory (LSTM) units was introduced to roller bearing fault diagnosis in [15]. In addition, many other DL methods have been proposed to build intelligent condition monitoring systems for bearings by analysing vibrational signals [16,17]. Inspired by those successful cases, an intelligent acoustic-based fault diagnosis on DL, is implemented for train bearing monitoring in this work. The approach taken here uses Graph Neural Networks.

Graph neural networks (GNN) were first proposed by Scarselli et al. [18], who aimed to build a neural network for data held in the graph domain based on graph theory. In the graph domain, the geometry structure of the data can provide additional information, including not only the values of the nodes but also the relationships between them [19]. Hence, more information can be provided in the graph domain than in a general data domain. Bruna et al. introduced the convolution operation into GNN based on spectral graph theory, and built the first graph convolutional network (GCN) model [20]. Compared with the conventional CNN method, GCN has advantages in dealing with the discriminative feature extraction of signals in the discrete spatial domain [21]. Up to now, the GCN method has been successfully applied to many research areas, such as website recommendation systems [22], electrocardiogram detection [23], etc. In this work, a deep graph convolutional network (DGCN) model is built and applied to form an intelligent acoustic-based fault diagnosis method.

The proposed DGCN model is constructed by multiple graph convolutional blocks [24], one fully connected layer, and one classification layer. The graph convolutional block includes one graph convolutional layer, one graph coarsening layer, and one graph pooling layer. Different from the convolution operator in the conventional CNN, the graph convolution layer used here uses a fast-localized spectral filter constructed according to a Chebyshev polynomial. In order to operate the pooling procedure after convoluting, a graph coarsening procedure is first used to group together similar vertices. Those vertices are then rearranged as a balanced binary tree before regular 1D pooling is undertaken. The effectiveness of the proposed intelligent system is verified using laboratory experiments comparing its performance with a range of conventional DL methods. The DGCN method is shown to outperform the conventional methods in terms of classification accuracy.

This paper is organised as follows: the deep graph convolutional network method is introduced in Section 2. In Section 3 the intelligent acoustic-based fault diagnosis using deep graph convolutional network is demonstrated. The experimental results, demonstrating the performance of the proposed method and comparing it to conventional techniques, are described in Section 4. The conclusions are then presented in the final section.

2. Graph convolutional network

A graph convolutional network has four main steps: input, convolution, coarsening, and pooling. (i) Graphs, as the input to a neural network, can represent the geometry and structure of data, and hence provide more information compared to more general data formats. (ii) To undertake a convolution operator on a graph, fast-localized filters are constructed based on the graph spectral theory and Chebyshev expansion. (iii) A graph coarsening procedure is used to group similar vertices together. (iv) For graph pooling, a rearrangement procedure is applied to the vertices by creating a balanced binary tree and then applying regular 1D pooling.

2.1. Graph representation

Undirected and connected graphs can be defined as $\mathcal{G} = (\mathcal{V}, \mathcal{E}, W)$ in which: $\mathcal{V}$ represents a set of vertices with the number of $|\mathcal{V}| = N$; $\mathcal{E}$ denotes the set of edges connecting these vertices; and $W \in \mathbb{R}^{n \times n}$ is an adjacency matrix demonstrating the connections between any two vertices. For example, $W_{i,j}$ is the weight of the edge $\mathcal{E}_{i,j}$ ($W_{i,j} = 0$, if there is no edge between vertices $\mathcal{V}_i$ and $\mathcal{V}_j$). Fig. 1 is an example of an undirected graph containing five vertices (a) and its adjacency matrix (b). In this paper, the Euclidean distance between two vertices is set to $W_{i,j}$, as shown in Eq. (1).

$$W_{ij} = \|\mathcal{V}_i - \mathcal{V}_j\| \tag{1}$$

In spectral graph analysis, the graph Laplacian is a key operation which is defined as shown in Eq. (2). In Eq. (2), I_n is the identity matrix; D is the diagonal degree matrix as shown in Eq. (3). The graph Laplacian L, which is a real symmetric matrix, can be operated by orthogonal decomposition as shown in Eq. (4). Hence, L
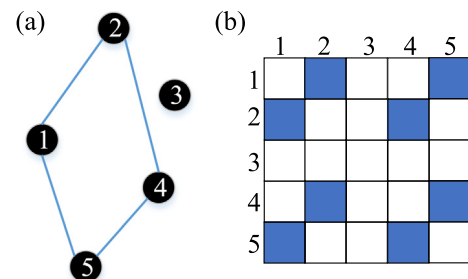

Fig. 1. An undirected graph and the corresponding adjacency matrix. (a) The connections of the five nodes (b) the adjacency matrix.

has a set of orthogonal eigenvectors $\{u_l\}_{l=0}^{n-1}$ and corresponding eigenvalues $\{\lambda_l\}_{l=0}^{n-1}$. In graph Fourier theory, the eigenvalues are the Fourier basis and are the frequencies of the graph.

$$L = I_n - D^{-1/2}WD^{-1/2} \tag{2}$$

$$d_i = \sum_{j=1, j\neq i}^{N} W_{ij} \tag{3}$$

$$L = U\Lambda U^T \tag{4}$$

where $\Lambda = \text{diag}([\lambda_0, \lambda_1, \cdots, \lambda_{n-1}])$ and $U = [u_0, u_1, \cdots, u_{n-1}]$.

A graph $x : \mathcal{V}(v_1, v_2 \cdots, v_N) \rightarrow \mathbb{R}^N (x_1, x_2 \cdots, x_N)$ defined on the i-th vector of x represents the i-th vertex value. The graph Fourier transform of x is defined in Eq. (5).

$$\widehat{x} = \sum_{i=1}^{N} u_l(i)^* x(i) = U^T x \tag{5}$$

The inverse graph Fourier transform is defined as shown in Eq. (6).

$$x = \sum_{i=0}^{N-1} \widehat{x}(i)^* u_l(i) = U\widehat{x} \tag{6}$$

where $\widehat{x}$ is the representation of the graph signal x in the Fourier domain.

2.2. Convolution operation for graph signals

The general convolution operation cannot be directly applied to graphs. However, a generalization method based on the graph Laplacian can be used to conduct convolution on graphs [25], as shown in Eq. (7). According to Eq. (4) and Eq. (7), graph convolution can be expressed as Eq. (8).

$$y = g_\theta(L)x \tag{7}$$

$$y = Ug_\theta(\Lambda)U^T x \tag{8}$$

The calculation of $g_\theta(\Lambda)$ is a difficult and time-consuming procedure [23]. To overcome this, a Chebyshev polynomial expansion can be used to simplify the calculation of $g_\theta(\Lambda)$ [24]. This is the approach followed in this work where $g_\theta(\Lambda)$ can be approximated using a Kth order Chebyshev polynomial as shown in Eq. (9).

$$g_\theta(\Lambda) = \sum_{k=0}^{K-1} \theta_k T_k(\Lambda) \tag{9}$$

where θ_k is a vector of Chebyshev coefficients and $T_k(x)$ is a recursive calculation as demonstrated in Eq. (10). Λ is a normalized version of Λ, which can be obtained according to Eq. (11). λ_{max} is the largest element of Λ. Hence, elements in Λ are in a range from -1 to 1.

$$\begin{cases} T_0(x) = 1, T_1(x) = x \\ T_k(x) = 2xT_{k-1}(x) - T_{k-2}(x), \quad k \geq 2 \end{cases} \tag{10}$$

$$\Lambda = \frac{2\Lambda}{\lambda_{max}} - I_n \tag{11}$$

According to Eq. (8) and Eq. (9), the graph convolution operation can be rewritten as Eq. (12).

$$y = \sum_{k=0}^{K-1} U \begin{bmatrix} \theta_k T_k(\lambda_0) & \cdots & 0 \\ \vdots & \ddots & \vdots \\ 0 & \cdots & \theta_k T_k(\lambda_{N-1}) \end{bmatrix} U^T x = \sum_{k=0}^{K-1} \theta_k T_k(L)x \tag{12}$$

where $L = 2L/\lambda_{max} - I_n$.

In GCNs which include multiple graph convolution layers, the jth output features of a sample s are given by Eq. (13).

$$y_{s,j} = \sum_{i=1}^{F_{in}} g_{\theta_{i,j}}(L)x_{s,j} \tag{13}$$

where $x_{s,j}$ are the input. $\theta_{i,j}$ are the trainable parameters of the jth layer, which are vectors of Chebyshev coefficients. In order to train the convolutional layers, a backpropagation algorithm is applied according to the two gradients in Eq. (14).

$$\begin{cases} \frac{\partial E}{\partial \theta} = \sum_{s=1}^{S} [\bar{x}_{s,j,0}, \cdots, \bar{x}_{s,j,K-1}]^T \frac{\partial E}{\partial y_{s,j}} \\ \frac{\partial E}{\partial x_{s,j}} = \sum_{j=1}^{F_{out}} g_{\theta_{i,j}}(L)\frac{\partial E}{\partial y_{s,j}} \end{cases} \tag{14}$$

where E is the energy loss for one batch with S samples. The gradients above can be efficiently computed by using a parallel architecture combined with tensor operations.

2.3. Graph coarsening

Before using a pooling operation for graphs, meaningful neighbourhoods on the graphs, i.e. similar vertices, must be clustered together. In this work, a multilevel clustering algorithm is used to obtain a coarser graph for each level in the GCN method. In the multilevel clustering algorithm, a greedy algorithm, also used in the weighted kernel k-means method, is applied to minimize the spectral clustering objective function and then for coarsening the graph. Comparing this with other spectral clustering methods, this method has advantages in terms of the quality of the results, speed of implementation, and memory usage [26].

Given $\mathcal{A}, \mathcal{B} \subset \mathcal{V}$ ($\mathcal{A}, \mathcal{B}$ are different sets in $\mathcal{V}$), weights between vertices in $\mathcal{A}$ and $\mathcal{B}$ can be defined as shown in Eq. (15).

$$\text{links}(\mathcal{A}, \mathcal{B}) = \sum_{i \in \mathcal{A}, j \in \mathcal{B}} W_{i,j} \tag{15}$$

The purpose of the graph clustering is to classify the graph into k sub-graphs, i.e. $\mathcal{V}_l, \cdots, \mathcal{V}_k \subset \mathcal{V}$. To achieve this, some standard graph clustering objectives were considered. The normalized cut objective, one of most commonly used methods, is applied as part of the proposed GCN method. The objective is expressed in Eq. (16).

$$\text{NCut}(\mathcal{G}) = \min_{\mathcal{V}_l, \cdots, \mathcal{V}_k} \sum_{c=1}^{k} \frac{\text{links}(\mathcal{V}_c, \mathcal{V} \setminus \mathcal{V}_c)}{\text{links}(\mathcal{V}_c, \mathcal{V})} \tag{16}$$

The minimization objective above is equivalent to maximizing with-in-cluster association relative to the size of the cluster. Using the weighted kernel k-means method, Eq. (16) can be expressed as a trace maximization problem, as in Eq. (17).

$$\max \left\{ \sum_{c=1}^{k} \frac{\text{links}(\mathcal{V}_c, \mathcal{V}_c)}{\text{degree}(\mathcal{V}_c)} = \sum_{c=1}^{k} \frac{x_c^T W x_c}{x_c^T D x_c} = \sum_{c=1}^{k} x_c^T W x_c \right\} \tag{17}$$

where x_c is the indicator vector of sub-graph c. W is the graph adjacency matrix. D is a diagonal degree matrix with $D_{i,j} = \sum_{j=1}^{n} W_{i,j}$, and $x_c = x_c/(x_c^T D x_c)^{1/2}$.

By maximizing Eq. (17) at each coarsening level, one unmarked vertex, $\mathcal{V}_i$, can be selected and it's matching neighbours, $\mathcal{V}_j$, identified. Each two matched vertices are then marked and the coarsened weights are set as the sum of their individual weights. The matching process is conducted iteratively until all vertices in the graph have been matched to. In this way, the number of vertices in one level can then be approximately divided in two.
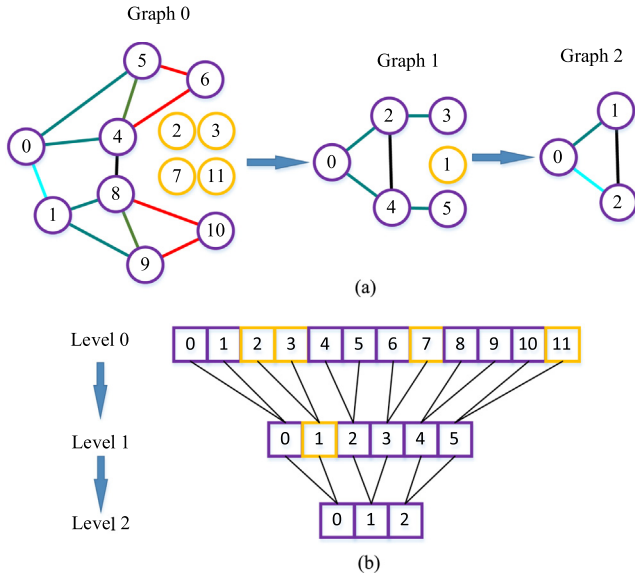
Fig. 2. Graph coarsening and pooling. (a) The coarsening operations for a graph with 12 vertices, (b) the pooling operations for the rearranged vertices.

2.4. Pooling operation for graphs

Although the vertices are clustered using graph coarsening, the marked vertices in each group are still in an arbitrarily order which blocks the pooling operation for graphs. In this work, a binary tree structure is constructed using the coarsened vertices. A rearrangement method is then used to sequence the vertices to be compatible with the pooling operation [24]. The arranged vertices can then be processed using a 1D pooling operation. The coarsening and pooling operations for a graph with 12 vertices are demonstrated in Fig. 2(a) and (b). In Fig. 2(a), a maximum pooling of size 4, i.e. size of 2 for each pooling, is applied to a graph with 12 vertices. Fig. 2(b) shows how the vertices are then rearranged to implement the pooling. The lines in Fig. 2(a) have the same colour if they connect matched vertices, otherwise they are shown with different colours. The vertex enumerators shown in the three levels

are allocated for each level, with the relationships shown in Fig. 2(b).

After the coarsening procedure described above, each vertex is normally matched and has two children (e.g. vertex 0 in level 1 in Fig. 2(b)). Some vertices, known as singletons, occur in the last level and only have one child. They occur when the child vertex cannot be matched in the coarsening process. Vertices that do not connect with any neighbours (e.g. vertex 1 in level 1 in Fig. 2 (b)) are known as fake vertices. A balanced binary tree can only be constructed if every vertex has two children. In this structure, one singleton and one normal vertex can form the two children of a vertex (e.g. vertex 0 in level 2 in Fig. 2(b)). Fig. 2(a) shows an original graph (Graph 0) where the input consists of 8 vertices in an arbitrarily order, and 4 fake vertices. By coarsening and rearranging the vertices to give those shown in Graph 1/Level 1, the pooling operation is rendered similar to a regular 1D pooling operation.

3. Intelligent acoustic-based fault diagnosis of roller bearings using deep graph convolution network

In this work, an intelligent acoustic-based fault diagnosis method is proposed using deep graph convolution network (DGCN). Acoustic signals are collected using a fixed microphone and then transformed into graphs, i.e. from the general data domain to the graph domain. The acoustic signals are divided into "samples", where each sample consists of 3600 points of the recorded signal. To generate graphs for the DGCN inputs, each acoustic sample, $\mathbf{x} = [x_1, x_2, \cdots, x_{3600}]$, is mapped into a matrix of size 60×60, where the first 60 points from sample $\mathbf{x}$ form the first row of the matrix. The matrices are then used to form graphs in which each matrix entry and it's 8 neighbouring points become vertices connected by edges. The edge weights are calculated from the vertex values as described in Eq.(1) The transformation procedure from the general data domain to the graph domain is demonstrated in Fig. 3.

After obtaining the graphs, multiple graph convolutional blocks are then used to extract abstract features. Each block includes one graph convolution layer, one graph coarsening layer, and a graph pooling layer. The graph convolutional layer is implemented according to the graph Laplacian and a Chebyshev polynomial.
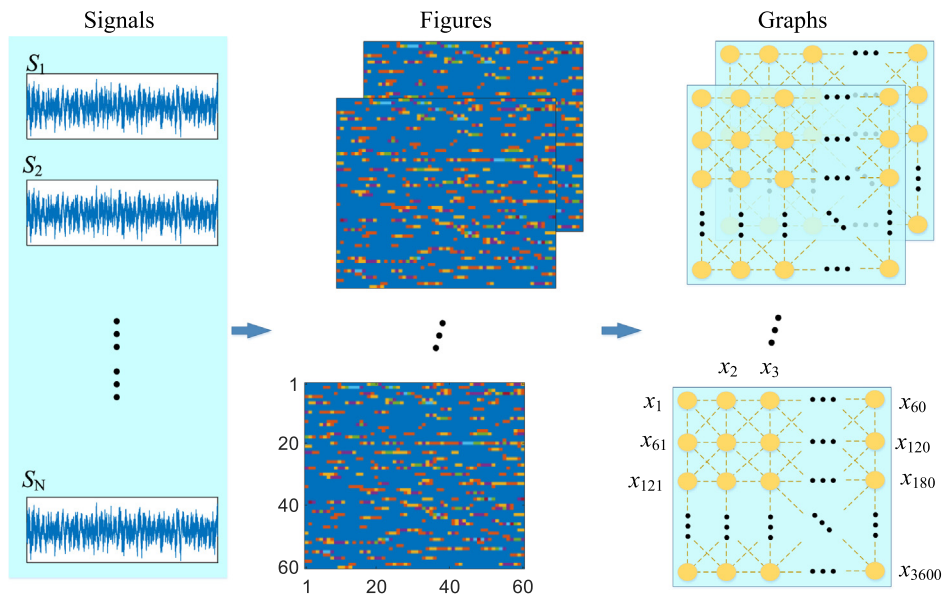

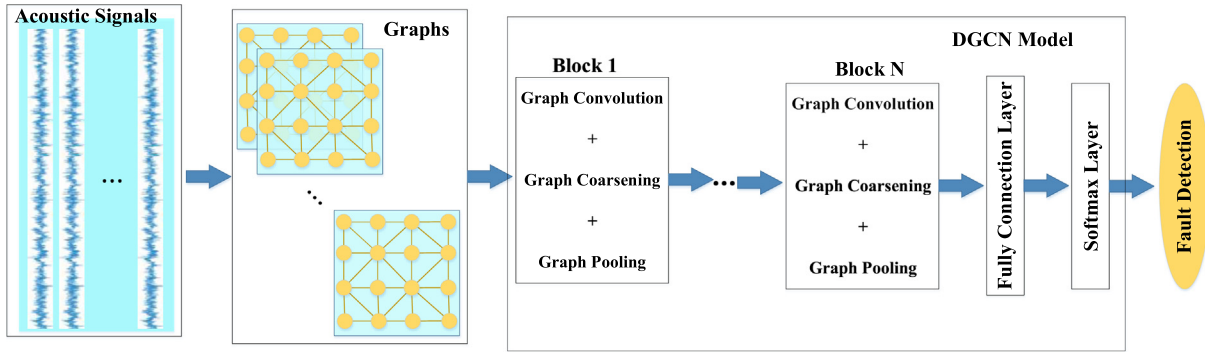**Fig. 3.** Schematic diagram for the construction of graphs.

Fig. 4. Flow chart of the intelligent acoustic-based fault diagnosis using deep graph convolution network.
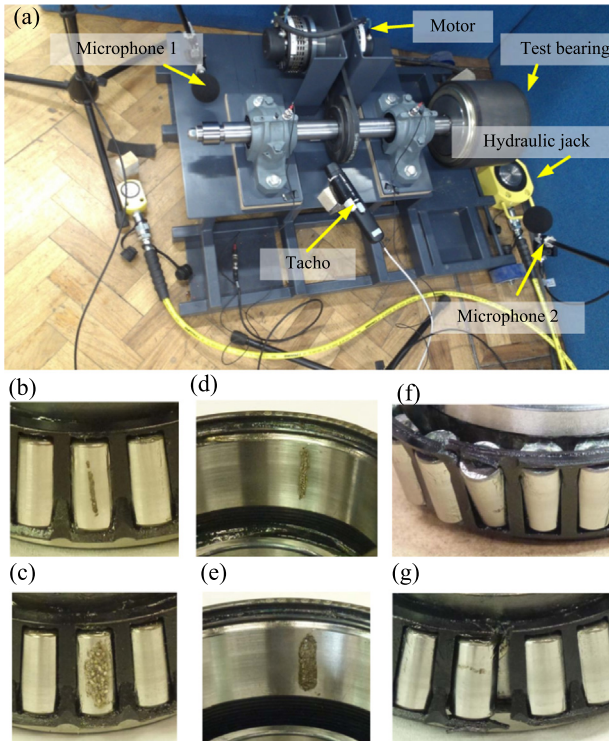

Fig. 5. Test rig and faulty bearings.

The graph coarsening layer is based on the weighted kernel *k*-means method and is used to cluster neighbourhoods together in a form compatible with the pooling layer. Following this rearrangement strategy, a graph pooling layer based on a 1D pooling operation is then applied to those clustered neighbourhoods. Multiple blocks can then be used iteratively to extract fault features from inputs. The learned features (i.e. the outputs of the blocks) are then fed into a fully connected layer and a SoftMax layer for fault detection. The performance of the DGCN approach is tested using testing samples in Section 4. A flow chart summarising the DGCN approach is presented in Fig. 4.

4. Experimental validation

4.1. Acoustic signal acquisition

The centre of this paper is to verify effectiveness of the proposed method for acoustic-based fault diagnosis. In this paper, a roller bearing test rig, shown in Fig. 5 (a), was used to collect the

Table 1
Fault conditions for test bearings.

Bearing ID	Description
H	Healthy statue without any fault
RF1	A minor scratch fault in one roller of bearing, shown in Fig. 4(b). The fault is inflicted using the electrical discharge engraver
RF2	A greater spalling fault in surface of one roller than that of RF1, shown in Fig. 4(c). A small rotary grindstone is used to remove surface material in the roller
OF1	A minor scratch fault in the outer race, shown in Fig. 4(d). Fault length is 2.9% of circumference. The fault is inflicted using the same method as RF2
OF2	Similar with OF1. But the scratch area in the outer race becomes widener and deeper, shown in Fig. 4(e). Fault length is 10% of circumference
CF1	The bearing cage cracked in one place, shown in Fig. 4(f). The damage is achieved by cutting and applying excess force with a screwdriver
CF2	The increased cage fault, shown in Fig. 4(g). The fault is inflicted using the same method as CF1

acoustic signals in the laboratory. The test rig supports multiple bearings, but in this case only a single bearing was used at any time and the data collected using Microphone 2. The type of test bearings used were 801023AB tapered roller bearings. 7 bearings were tested, including one healthy bearing, two bearings with outer race faults, two bearings with roller faults, and two bearings with cage faults. The faults present in the test bearings are shown in Fig. 5 (b)–(g), respectively. The fault details and the methods of artificially creating them are summarised in Table 1. Vertical load was added to the test bearing using a Hydraulic jack. In the experiments, the sampling frequency was 12500 Hz.

In this work, each fixed-speed and fixed-load recording from the test rig was divided up to form 600 "audio clips", where each clip is formed of 3600 data points. The time domain waveforms of the acoustic signals for both healthy and faulty bearings are shown in Fig. 6. The figure shows that the collected acoustic signals have serious harmonic interference. 80% of the audio clips are randomly selected to be training samples, and remaining samples are used as testing samples.

4.2. Parameter identification of DGCN

To identify the structure of the DGCN, i.e. the depth (D) and the width (W), experiments using healthy bearings (H) and bearings with roller faults (RF1 and RF2) were conducted at a speed of 500 RPM. A stepwise optimisation strategy was applied in the parameter selection procedure. The depth was first fixed as 1 (D1) and the width varied with the resulting accuracies shown in Table 2. From this, the width of the first layer, W_{D1}, is selected to
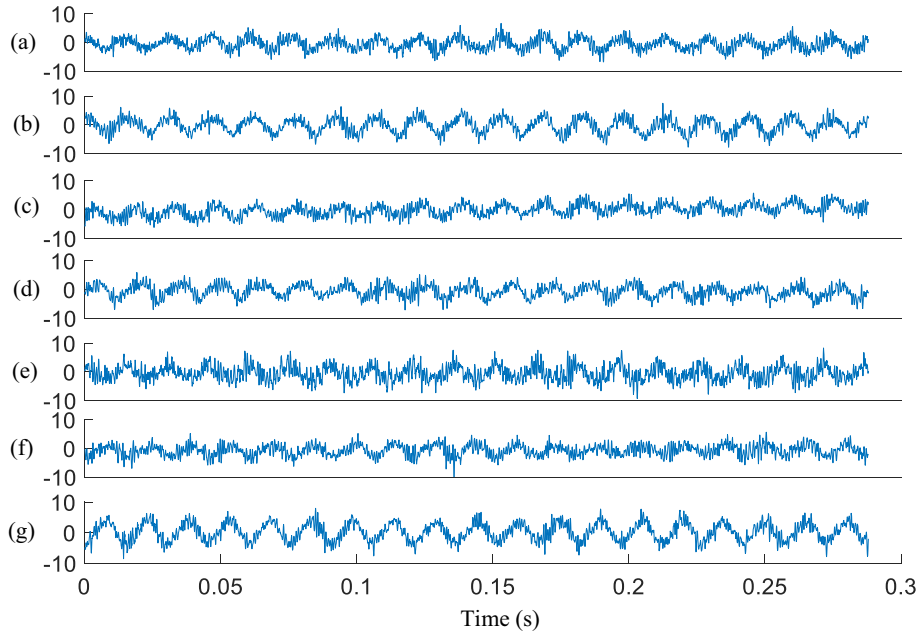
Fig. 6. Example time domain waveforms of the acoustic signals for both healthy (a) and faulty (b–g) bearings.

Table 2
DGCN performance for different structural parameters.

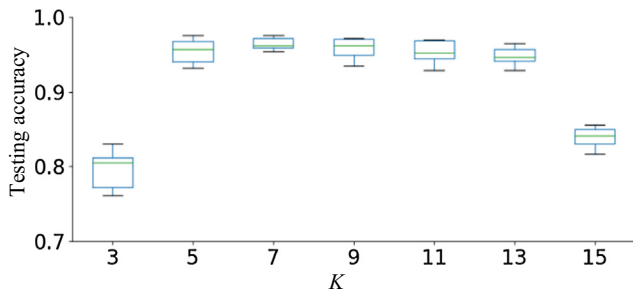| W_{D1}	32	64	128	256
Accuracy	78.81%	80.93%	80.08%	76.27
$W_{D1 \times D2}$	64×32	64×64	64×128	64×256
Accuracy	85.17%	86.86%	89.83%	90.25%
$W_{D1 \times D2 \times D3}$	$64 \times 256 \times 32$	$64 \times 256 \times 64$	$64 \times 256 \times 128$	$64 \times 256 \times 256$
Accuracy	95.76%	94.07%	90.25%	86.86%
$W_{D1 \times D2 \times D3 \times D4}$	$64 \times 256 \times 32 \times 32$	$64 \times 256 \times 32 \times 64$	$64 \times 256 \times 32 \times 128$	$64 \times 256 \times 32 \times 256$
Accuracy	93.13%	91.36%	88.53%	84.79%

Fig. 7. Accuracy results for different kernel lengths.

be 64. After fixing the width of the first layer, a similar experiment is conducted to identify an appropriate value for the width of the second layer (D2). The experiment shows that the best performance is obtained when the widths of the first two layers, $W_{D1 \times D2}$, are selected as 64×256. Experiments are conducted repeatedly using this format to obtain the final structure parameters with the depth ultimately being selected as 3 and the corresponding widths as 64, 256, and 32.

The order number of the Chebyshev polynomial expansion in Eq. (9), known as kernel length K, is another core parameter for the DGCN model and its value directly affects the classification result. To select the optimal value of kernel length, a comparison
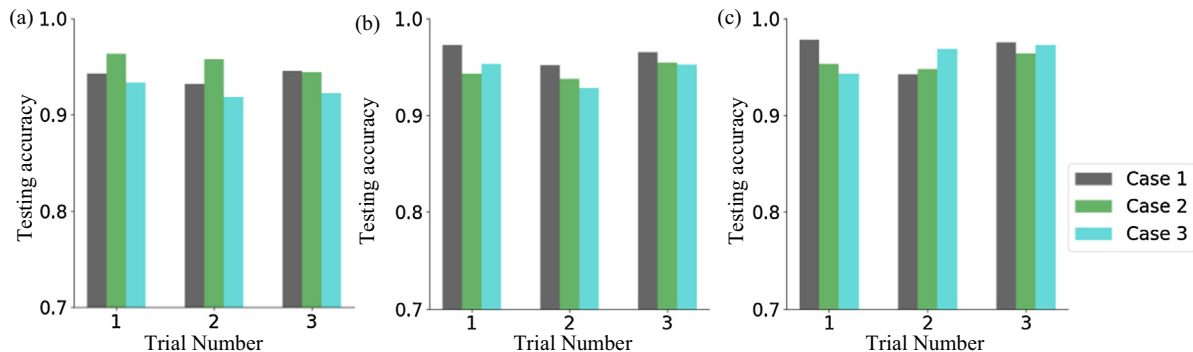

Fig. 8. Classifier accuracy results for bearing classification of 3 fault cases at varying speeds: (a) 400 rpm, (b) 500 rpm and (c) 600 rpm.
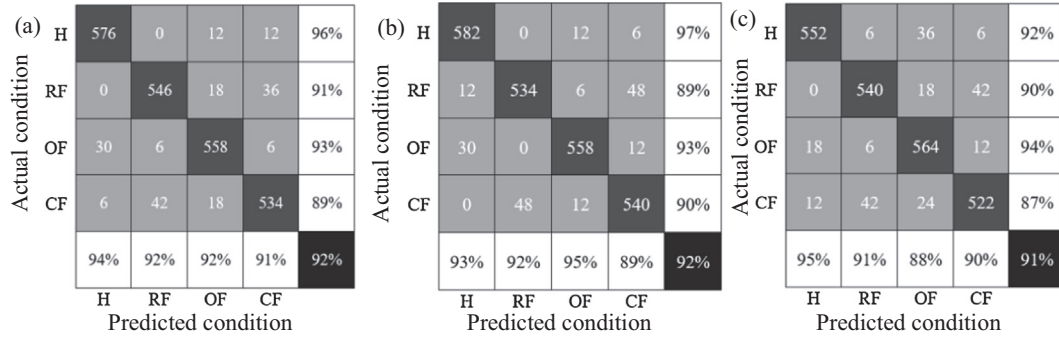
Fig. 9. Confusion Matrixes showing the classification results using the DGCN model: (a) 400 rpm, (b) 500 rpm and (c) 600 rpm.
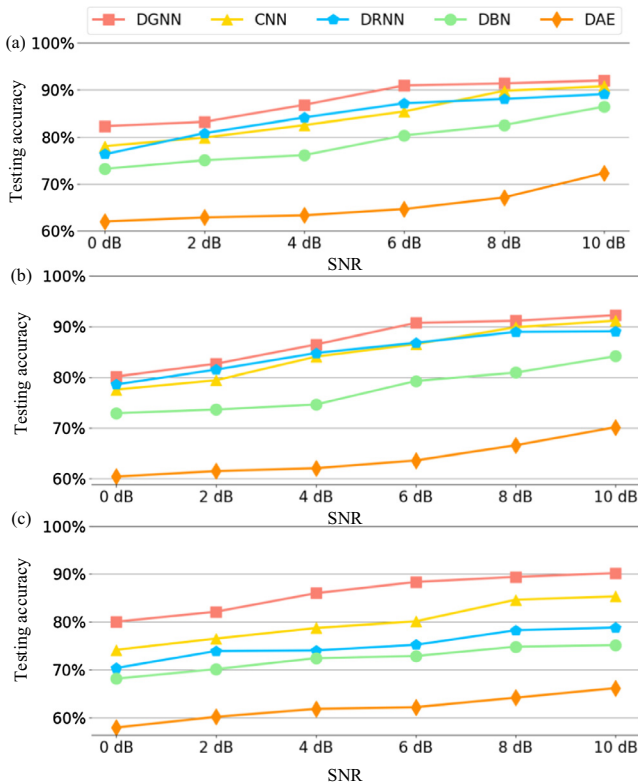

Fig. 10. Testing accuracy results for different classification methods with varying SNR at (a) 400 rpm, (b) 500 rpm and (c) 600 rpm.

experiment was conducted using the proposed method and varying the kernel length. The boxplot in Fig. 7 shows the comparison results. The figure shows that the median value of the testing accuracy increases as the kernel length is increased from 3 to 7 and then the decreases as the kernel length is further increased from 7 to 15. Hence, the best performance is obtained with a kernel length of 7, and this is used in the DGCN model.

4.3. Detection of different fault severities

Under real operation, the speed of roller bearings varies with time. Hence, the DGCN's robustness for varying speed was tested using a further comparison experiment. In the experiment, acoustic signals were collected from testing bearings operating at 400 rpm, 500 rpm and 600 rpm. Three fault cases were included in the experiment: Case 1 used bearings H (healthy), RF1 and RF2 (both roller faults); Case 2 used bearings H (healthy), OF1

and OF2 (both outer race faults); and Case 3 used bearings H (healthy), CF1 and CF2 (both cage faults). Three trials were conducted for each fault case in order to verify the stability of the proposed model. The comparison results are shown in Fig. 8. The figure shows that good performance can be obtained from the DGCN model regardless of rotational speed. Furthermore, the stability of the proposed model is verified.

4.4. Detection of different fault types

To further test the effectiveness of the DGCN model, an experiment was conducted using test bearings with different faults and at different speeds. In the experiment, bearings H, RF1, OF1 and CF1 were selected as the test bearings. The confusion matrixes of the classification results are shown in Fig. 9. The classification accuracy shown in Fig. 9 demonstrates that the DGCN model can be used to detect multiple kinds of faults effectively. The confusion matrixes, and in particular the overall accuracy, are similar when samples are collected at different operating speeds. There is a slight variation in overall accuracy above 600 rpm, this is mainly because the background noise in the collected acoustic signal becomes more significant with the increase in speed.

4.5. Detection with different levels of background noise

Significant background noise is usually included in the acoustic data. The level of this noise directly affects the performance of any classification model. Hence, the robustness of the system against noise is important. To test the performance of the DGCN model in relation to noise, a further comparison experiments was conducted using the test bearings H, RF1, OF1 and CF1, operating at different speeds. Multiple deep learning algorithms were then used to classify the different faults and their performance compared to the proposed method.

The first comparison method used was the conventional convolutional neural network (CNN). This was constructed using three convolutional blocks (convolution layer + pooling layer) to extract features from the raw acoustic data. The other parameters in the CNN are the same as that in reference [9]. The second comparison method uses a deep recurrent neural network (DRNN) [15]. The third one comparison method was a deep belief network (DBN) constructed from three Boltzmann machine layers and used to automatically extract features [27]. The final comparison method used a deep autoencoder (DAE) with three neural layers to extract features [28]. Additive White Gaussian Noise (AWGN) with different levels was added to the collected acoustic signals to vary the signal-to-noise ratio (SNR) from 0 dB to 10 dB. The comparison experiment was conducted at different speeds (400, 500 and 600 RPM). The results of the comparison experiment are shown in Fig. 10. The figure shows that for all of the classifiers, the accuracy
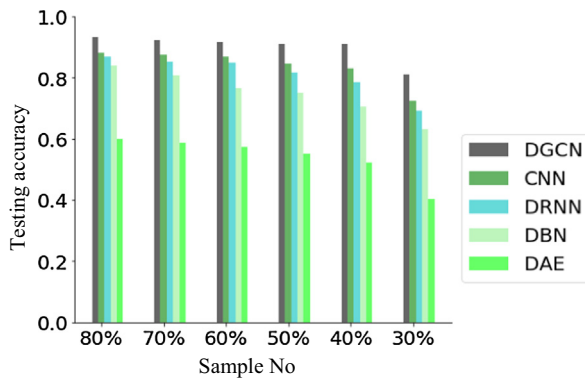
Fig. 11. Testing accuracy results for different classifiers based on different dataset sizes.

decreases as the background noise increases. The figure also shows that the DGCN model has the best performance of all the methods compared for all of the speeds considered.

4.6. Detection with different sample sizes

In real operating conditions it is often difficult to collect large quantities of data, and as such classification systems that can operate with smaller datasets may be preferable. The accuracy of most classifiers is sensitive to the size of their training dataset. To test the performance of the DGCN model against the other learning algorithms considered in Section 4.5 in the case of limited datasets, a further comparison experiment was conducted using testing bearings H, RF1, OF1 and CF1 operating at 500 rpm. The classifier results are shown in Fig. 11. The figure shows that the testing accuracy for all methods decreases as the number of training samples is reduced. The proposed DGCN method is shown to produce the most accurate classification result compared to the other methods considered. This is largely due to its capability for learning the geometric information of graphs. Although the DGCN model can obtain the best result for each dataset size, its classification accuracy still follows the trends of all of the methods – i.e. decreasing with dataset size. All of the methods show a significant decrease in accuracy as the training proportion falls below 30%.

5. Conclusions

In this work, an intelligent acoustic-based fault diagnosis using deep graph convolution networks has been proposed and demonstrated to be suitable for identifying roller bearing faults. In the approach, the collected acoustic signals are transformed into graphs, i.e. from the general data domain to the graph domain. The training sets of graphs, as inputs, are then fed into the deep graph convolution network which includes multiple feature extraction blocks, one fully connected layer, and a SoftMax layer. For the feature extraction blocks in the DGCN model, there are three core procedures: graph convolution, coarsening, and pooling operations based on spectral graph theory. Finally, the testing sets of graphs are used to validate the performance of the trained DGCN model. The performance of the proposed scheme has been verified under a range of scenarios using multiple experiments and comparisons with other methods. The methods have been considered for their performance in terms of: consistency, stability with speed, fault type, fault severity, noise tolerance, and dataset size. The following conclusions are obtained through consideration of the experimental results:

(1) The graphs constructed using vertices and edges can provide more information for training the DL model. Hence, the results of the experiments demonstrate that The DGCN method is superior to conventional DL methods for identifying different fault severities and different kinds of bearing faults.
(2) The graph construction methods described work well in the proposed approach and in comparison to a range of other popular methods as demonstrated. However, there are many other methods, including different geometry structures, weighted methods, etc. and so further comparative studies are required.
(3) It has been shown that the results of the proposed scheme can be obtained using the collected acoustic signals from the test rig in the lab. The intelligent method has, however, not yet been validated using real-world data.

CRediT authorship contribution statement

Dingcheng Zhang: Writing - original draft, Methodology, Software, Validation, Formal analysis. **Edward Stewart:** Supervision, Writing - review & editing. **Mani Entezami:** Supervision, Investigation, Data curation. **Clive Roberts:** Supervision, Resources, Visualization, Project administration. **Dejie Yu:** Conceptualization.

Declaration of Competing Interest

The authors declare that they have no known competing financial interests or personal relationships that could have appeared to influence the work reported in this paper.

Acknowledgements

References

[1] X. Zhang et al., Acoustic performance of a semi-closed noise barrier installed on a high-speed railway bridge: measurement and analysis considering actual service conditions, Measurement 138 (2019) 386–399.
[2] N. Baydar, A. Ball, Detection of gear failures via vibration and acoustic signals using wavelet transform, Mech. Syst. Sig. Process. 17 (4) (2003) 787–804.
[3] A. Glowacz, Fault diagnosis of single-phase induction motor based on acoustic signals, Mech. Syst. Sig. Process. 117 (2019) 65–80.
[4] A. Glowacz et al., Early fault diagnosis of bearing and stator faults of the single-phase induction motor using acoustic signals, Measurement 113 (2018) 1–9.
[5] C. Wang et al., Doppler Effect removal based on instantaneous frequency estimation and time domain re-sampling for wayside acoustic defective bearing detector system, Measurement 50 (2014) 346–355.
[6] D. Zhang et al., Adaptive fault feature extraction from wayside acoustic signals from train bearings, J. Sound Vib. 425 (2018) 221–238.
[7] X. Guo, L. Chen, C. Shen, Hierarchical adaptive deep convolution neural network and its application to bearing fault diagnosis, Measurement 93 (2016) 490–502.
[8] R. Liu et al., Artificial intelligence for fault diagnosis of rotating machinery: a review, Mech. Syst. Sig. Process. 108 (2018) 33–47.
[9] T. Ince et al., Real-time motor fault detection by 1-D convolutional neural networks, IEEE Trans. Ind. Electron. 63 (11) (2016) 7067–7075.
[10] M. Zhao et al., Deep residual networks with dynamically weighted wavelet coefficients for fault diagnosis of planetary gearboxes, IEEE Trans. Ind. Electron. 65 (5) (2018) 4290–4300.
[11] S. Wang et al., A data indicator-based deep belief networks to detect multiple faults in axial piston pumps, Mech. Syst. Sig. Process. 112 (2018) 154–170.
[12] W. Zhang et al., A deep convolutional neural network with new training methods for bearing fault diagnosis under noisy environment and different working load, Mech. Syst. Sig. Process. 100 (2018) 439–453.
[13] H. Shao et al., Rolling bearing fault feature learning using improved convolutional deep belief network with compressed sensing, Mech. Syst. Sig. Process. 100 (2018) 743–765.
[14] F. Jia et al., Deep neural networks: a promising tool for fault characteristic mining and intelligent diagnosis of rotating machinery with massive data, Mech. Syst. Sig. Process. 72 (2016) 303–315.

[15] H. Jiang et al., Intelligent fault diagnosis of rolling bearings using an improved deep recurrent neural network, Meas. Sci. Technol. 29 (6) (2018) 065107.

[16] M. Gan, C. Wang, Construction of hierarchical diagnosis network based on deep learning and its application in the fault pattern recognition of rolling element bearings, Mech. Syst. Sig. Process. 72 (2016) 92–104.

[17] W. Mao et al., Online sequential prediction of bearings imbalanced fault diagnosis by extreme learning machine, Mech. Syst. Sig. Process. 83 (2017) 450–473.

[18] F. Scarselli et al., The graph neural network model, IEEE Trans. Neural Networks 20 (1) (2009) 61–80.

[19] A. Ortega et al., Graph signal processing: overview, challenges, and applications, Proc. IEEE 106 (5) (2018) 808–828.

[20] J. Bruna et al., Spectral networks and locally connected networks on graphs, 2013. arXiv preprint arXiv:1312.6203.

[21] F.P. Such et al., Robust spatial filtering with graph convolutional neural networks, IEEE J. Sel. Top. Signal Process. 11 (6) (2017) 884–896.

[22] R. Ying et al., Graph Convolutional Neural Networks for Web-Scale Recommender Systems, 2018. arXiv preprint arXiv:1806.01973.

[23] T. Song et al., EEG emotion recognition using dynamical graph convolutional neural networks, IEEE Trans. Affective Comput. (2018).

[24] M. Defferrard, X. Bresson, P. Vandergheynst, Convolutional neural networks on graphs with fast localized spectral filtering, Advances in Neural Information Processing Systems, 2016.

[25] D.I. Shuman et al., The emerging field of signal processing on graphs: Extending high-dimensional data analysis to networks and other irregular domains, IEEE Signal Process Mag. 30 (3) (2013) 83–98.

[26] I.S. Dhillon, Y. Guan, B. Kulis, Weighted graph cuts without eigenvectors a multilevel approach, IEEE Trans. Pattern Analysis Mach. Intell. 29 (11) (2007).

[27] M. Ma, C. Sun, X. Chen, Discriminative deep belief networks with ant colony optimization for health status assessment of machine, IEEE Trans. Instrum. Meas. 66 (12) (2017) 3115–3125.

[28] H. Shao et al., A novel deep autoencoder feature learning method for rotating machinery fault diagnosis, Mech. Syst. Sig. Process. 95 (2017) 187–204.